AIP | Applied Physics Letters

Engineering 180° ferroelectric domains in epitaxial PbTiO3 thin films by varying the thickness of the underlying (La,Sr)MnO3 layer

L. Jin, C. L. Jia, and I. Vrejoiu

Citation: Applied Physics Letters **105**, 132903 (2014); doi: 10.1063/1.4897144
View online: http://dx.doi.org/10.1063/1.4897144
View Table of Contents: http://scitation.aip.org/content/aip/journal/apl/105/13?ver=pdfcov
Published by the AIP Publishing

Engineering 180° ferroelectric domains in epitaxial $PbTiO_3$ thin films by varying the thickness of the underlying (La,Sr)MnO_3 layer

L. Jin,[1,a)] C. L. Jia,[1,2] and I. Vrejoiu[3]
[1]*Peter Grünberg Institute and Ernst Ruska-Centre for Microscopy and Spectroscopy with Electrons, Research Centre Jülich, D-52425 Jülich, Germany*
[2]*International Center for Dielectric Research, Xi'an Jiaotong University, Xi'an 710049, China*
[3]*Max Planck Institute for Solid State Research, Heisenbergstr. 1, D-70569 Stuttgart, Germany*

(Received 16 August 2014; accepted 20 September 2014; published online 30 September 2014)

Epitaxial ferroelectric thin films of $PbTiO_3$ (PTO) grown on top of nominally $La_{0.7}Sr_{0.3}MnO_3$ (LSMO) submicron hillocks on Nb-doped $SrTiO_3$ (100) substrate were investigated by means of scanning transmission electron microscopy. 180° ferroelectric domains were observed in the ***c***-axis oriented PTO films. The formation and configuration of ferroelectric domains and domain walls were found to exhibit strong correlation with the thickness of the underlying LSMO hillocks. The domain walls start at the locations of the hillocks where the LSMO layer has a thickness of about 3 nm. Our results demonstrate that controlling the thickness variation (shape) of the LSMO hillocks can manipulate the position and density of the ferroelectric domain walls, which are considered to be the active elements for future nanoelectronics. © *2014 AIP Publishing LLC*.
[http://dx.doi.org/10.1063/1.4897144]

Perovskite oxides with ABO_3 structure possess a wide range of properties, such as dielectricity, ferroelectricity, piezoelectricity, superconductivity, colossal magnetoresistance, and multiferroicity, which have attracted a long-term research interest.[1–7] These materials provide for studies of abundant physical phenomena. In the meantime, they have also shown a variety of (potential) applications for future information technology, e.g. in capacitors, non-volatile memories, solar cells, and so on.[7–9] In order to exploit the properties as well as to realize applications, these materials are usually used in the form of films or multilayers (consisting of different ABO_3 components), whose structures and performances could be manipulated by composition, components, and substrate strain by epitaxial growth.[6]

$PbZr_xTi_{1-x}O_3$ (PZT) is an important ferroelectric material having large room temperature polarization and piezoelectric coefficients. PZT is often deposited epitaxially on a $SrTiO_3$ (STO) single crystal substrate, with or without a bottom electrode like (La,Sr)MnO_3 or $SrRuO_3$.[10–14] Lots of works[11–13] have been performed to study the influence from the substrate and electrode on the properties of PZT layers. Stripes of 180° domains have been reported for thin films of $PbTiO_3$ (PTO, i.e., PZT for $x = 0$) grown on the STO substrate,[15,16] whereas the film exhibits a monodomain state when a $SrRuO_3$ or (La,Sr)MnO_3 layer was used as bottom electrode.[10,12] To reduce the depolarization field, flux-closure domains form in the area between 180° domain wall (DW) of PZT and insulating STO substrate, and have been studied with a precision of a few picometers by applying negative spherical aberration (Cs) imaging.[11] The physical properties and structures of DWs in ferroelectrics and multiferroics have been studied theoretically[17–21] and experimentally[11,22–29] in great detail. It was often found that the DWs possess properties different from the domain bulk. Conductivity was measured at DWs including charged 180° DWs.[26,27,30] The presence of DWs further increases the photovoltaic response significantly because of the electrical fields existing within the narrow DWs.[28,29] The properties exhibited by DWs stimulate great interest in experimentally exploring the structure and formation of DWs and their applications in future nanoelectronics.[31] In addition, the physical properties of ferromagnetic metallic (La,Sr)MnO_3 could be also manipulated by the neighboring ferroelectric film, which implies that a strong coupling may exist between the ferroelectric and correlated electron oxides.[14]

In this letter, we report on the formation of ordered 180° domains in PTO thin film that appears to be related to the thickness variations of (La,Sr)MnO_3 submicron structures. A characteristic maximum thickness of the (La,Sr)MnO_3 of about 3 nm was determined by high spatially resolved (scanning) transmission electron microscopy ((S)TEM) together with electron energy loss spectroscopy (EELS), on which PTO possesses downward polarization. The strong dependence provides us a possible way to control the position and density of domains and DWs in ferroelectric films, which are considered as a highly potential element in future nanoelectronics.

Heterostructures with about 50 nm thick PTO film and submicron sized nominally $La_{0.7}Sr_{0.3}MnO_3$ (LSMO) hillock structures were epitaxially deposited on a semi-conductive Nb-doped STO (Nb-STO) (100)-oriented substrate by pulsed-laser deposition. The LSMO hillocks were grown at ~600 °C through a stencil mask, which was mechanically attached to the surface of the Nb-STO substrate. After removing the stencil, the LSMO/Nb-STO structure was reheated to 585 °C and then a 50 nm thick PTO film was deposited on the same area (see Ref. 12 for detailed information). Figure 1 shows a scanning electron microscopy image of the hillocks with a diameter of about 1 μm. The heterostructures were probed by piezoresponse force microscopy (PFM) with an MFP-3D Asylum Research scanning probe microscope with an external lock-in amplifier (SRS830 DSP

[a)]Author to whom correspondence should be addressed. Electronic mail: l.jin@fz-juelich.de

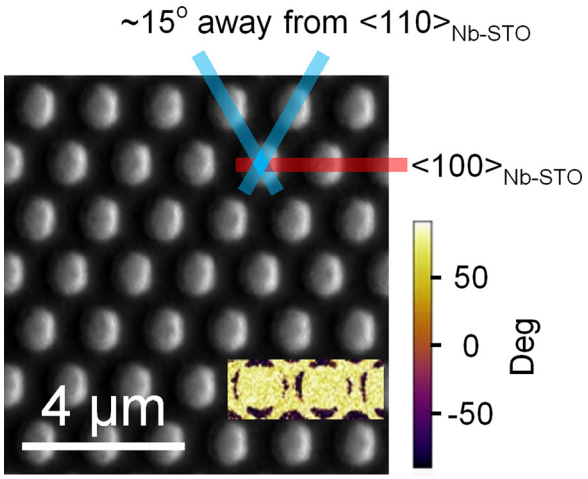

FIG. 1. Representative scanning electron micrograph of the sample. The lines indicate how FIB lamellae were cut with crystallographic orientations of $\langle 100\rangle_{\text{Nb-STO}}$ and $\langle 110\rangle_{\text{Nb-STO}}$. Inset is the out-of-plane piezoresponse force microscopy image. The bright contrast corresponds to upward polarization and dark contrast to the downward polarization of the PTO film.

Stanford Research Systems) prior to the microstructural research. The out-of-plane PFM image is shown as inset of Figure 1. In the PFM image, the bright contrast corresponds to upward polarization and the dark contrast to downward polarization of the PTO layer. In between the LSMO hillocks, where the tetragonal PTO layer grows *c*-axis oriented on the Nb-STO substrate, the polarization is uniformly pointing upwards. Directly on top of the LSMO dot and partly on their wedge-like edges, the polarization is oriented upward as well. However, around the LSMO hillocks, in regions of 50–200 nm width, the polarization of the PTO film turns to downward orientation.

Cross sectional lamella specimens across the areas including the hillocks were prepared for (S)TEM studies by focused ion beam (FIB) milling with an FEI Helios Nanolab 400s dual-beam system. More than 16 lamellae were cut with crystallographic orientations of $\langle 100\rangle_{\text{Nb-STO}}$ and $\langle 110\rangle_{\text{Nb-STO}}$ for statistic investigation. The geometry of the lamellae is schematically shown by thick lines in Figure 1.

The FIB-prepared lamellae were polished by 500 eV argon ion-beam (Fischione Nanomill, Model 1040) to remove the damaged layers introduced by FIB milling. High-resolution (HR) TEM investigation was performed on an FEI Titan 80–300 transmission electron microscope with a Cs correction system for the objective lens, running at an acceleration voltage of 300 kV. Investigations based on STEM techniques, including annular bright-field (ABF) imaging, high-angle annular dark-field (HAADF) imaging, and StripeSTEM,[32] were carried out on an FEI Titan 60–300 PICO microscope (working at 200 kV) equipped with a high-brightness field emission gun, a monochromator unit, a Cs probe corrector, and a Cs-Cc (chromatic aberration) image corrector, and on an FEI Titan 80–300 scanning transmission electron microscope at 300 kV with a probe Cs-correction system. EELS data processing were performed in Gatan DigitalMicrograph software.

Figure 2(a) shows an ABF image including one and a half LSMO hillocks underneath a continuous PTO film with thickness of approximately 50 nm. In Figure 2(a), it can be seen from the image contrast that two domains (denoted as D2 and D4) with width of about 100 nm, as indicated by the arrows, are located upon the edge region of the LSMO hillocks, which correspond to the regions of the annular-shaped domains with negative PFM phase (dark contrast) in inset of Figure 1. The other domains in the PTO film, D1 and D5 (on top of the LSMO hillocks), and D3 (mainly directly on top of the Nb-STO substrate), show a positive phase (bright contrast) in inset of Figure 1. A magnified view of the area corresponding to domain D2 is shown in Figure 2(b). In this image, three domains D1, D2, and D3 can be clearly seen in the PTO layer separated by two DWs, as marked by black arrows. The DWs are slightly inclined, thereby exhibiting a dark contrast in the ABF image. Beneath domain D1, a contrast of wedge-shaped ultra-thin layer can be recognized, as marked by the yellow arrow in Figure 2(b), extending into the central domain D2. This is the foot tail of the LSMO hillock.

The atomic structure of the domains has been studied by atomic-resolution ABF imaging. As a representative result, Figure 2(c) shows an image of domain D3. A unit-cell

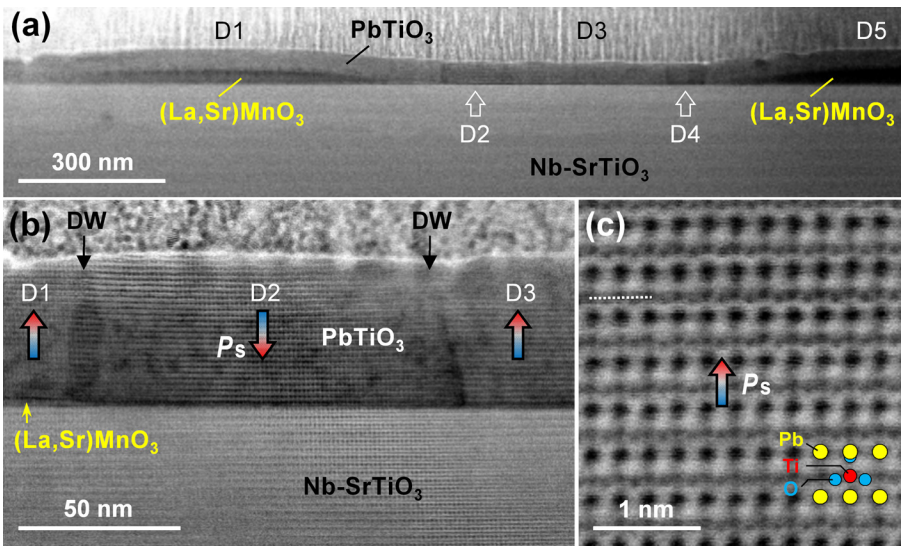

FIG. 2. Annular bright-field images showing the domain patterns at different magnifications: (a) low, (b) medium, and (c) atomically resolved. The semi-convergent angle of the electron beam was 21.4 mrad, while the ABF collection angle was 12-24 mrad. Superimposition in (c) is the single unit cell model of PTO along [110] axis.

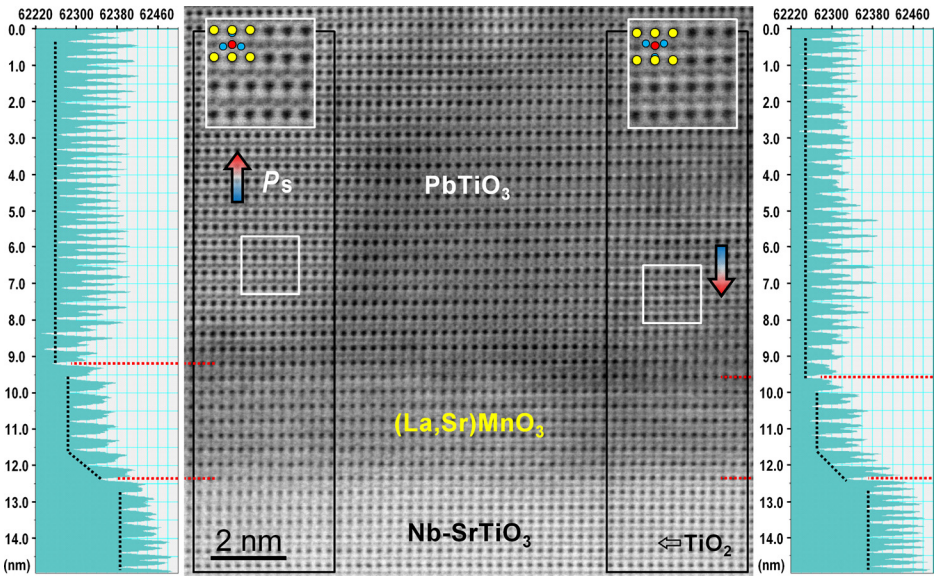

FIG. 3. Annular bright-field image (central panel) showing the atomic details of the region close to a 180° domain wall. Insets are magnifications of the square regions showing upward and downward $\boldsymbol{P}_s$, respectively. Corresponding intensity line profiles in the left and right panels showing the thickness of underlying LSMO layer. The dotted lines are guide for the eyes.

atomic model overlies the lower right corner of the image. The image was recorded along the [110] direction. In this direction, all of the columns, PbO, Ti, and O, are revealed as dark dots under a bright background.[33] The displacement of the O atoms (denoted by blue symbol) relative to the Ti atoms (denoted by red symbol) is evident, resulting in a zigzag feature of the TiO_2 plane (marked by dot line): the O atoms are shifted downward with respect to the Ti atoms along the PTO [001] direction. The relative displacements lead to a separation of the center of the negative charge of O from that of the positive charge of the metal cations, and thus to electrical dipoles. The direction of the spontaneous polarization vector $\boldsymbol{P}_s$ is defined (as the direction from net negative to net positive charge) to be upward for D3. The directions of $\boldsymbol{P}_s$ for D1 (upward) and D2 (downward) were also determined (see Figure 3), which shows exactly the same polarization configuration (Figure 2(b)) as that observed by PFM in inset of Figure 1.

The structural details in the vicinity of the left DW are presented in the central panel of Figure 3. All three components of the heterostructure (i.e., PTO film, LSMO edge, and STO substrate) were atomically resolved. In the STO substrate, the TiO_2 plane (indicated by the horizontal arrow) is indeed straight as expected for the cubic perovskite structure, which acts as a reference for determining the atom displacements and thus for determining $\boldsymbol{P}_s$ in PTO domains. Two insets show the magnifications of the square regions in domains D1 and D2, respectively. The polarization vector changes direction by 180° across the DW from D1 to D2 as clearly seen by the opposite Ti-O relative shifts, which means the left DW is a 180° DW. Same investigation has been applied to the right DW resulting in also a 180° type of wall.

The occurrence of the 180° DWs is found to closely relate to the positions of the LSMO hillocks. It is of great importance to determine the thickness of the LSMO layer at these positions. The thickness of the LSMO layer was determined by StripeSTEM technique.[32] Figure 4 represents a StripeSTEM dataset containing a HAADF image and a simultaneously collected EELS-stack image from a nearly uniform LSMO layer. The stack image consists of 93 spectra; each spectrum was acquired within 2 s and calibrated according to the Ti-$L_{2,3}$ edge of the Nb-STO substrate.[34] The energy resolution of EELS is about 0.8 eV defined as the full width at half maximum of the zero loss peak. For better illustration, the Ti-$L_{2,3}$, Mn-L_3, and La-$M_{4,5}$ core-shell excitations are displayed individually in false color. The layer-by-layer modulated intensities of Ti-$L_{2,3}$, Mn-L_3, and La-$M_{4,5}$ reveal that the EELS-stack image in StripeSTEM demonstrates monolayer resolution along the slow scanning direction (the film normal). The oscillation of O signal (not shown) is relatively weak, especially in the STO substrate, which has no effects on determination of the LSMO layer thickness. The modulations in B-site Ti-$L_{2,3}$ and Mn-L_3 are shifted by a[001]/2 from that of A-site La-$M_{4,5}$, in agreement with the perovskite structure. Therefore, by counting the

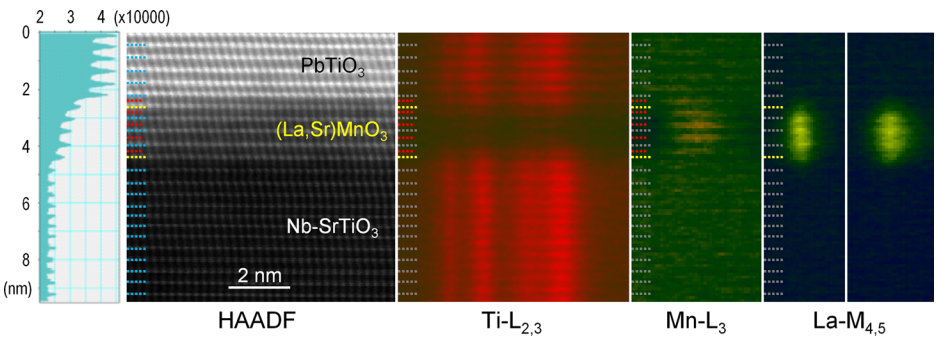

FIG. 4. A StipeSTEM dataset including a HAADF image and EELS-stack images of Ti-$L_{2,3}$ (455.5–471.5 eV), Mn-L_3 (639.7–648.7 eV), and La-$M_{4,5}$ (836.9–842.5 eV and 852.9–858.9 eV). The probe semi-convergent angle, the inner HAADF detector angle, and the collection angle of the spectrometer were 25, 70, and 21 mrad, respectively. The left panel showing the line profile of HAADF image with an integration window of ~2.76 nm.

modulated signals of A-site La-$M_{4,5}$ and B-site Mn-L_3 we determined the thickness of LSMO layer as five perovskite unit cells.

As direct comparison, the intensity profile of the HAADF image is also shown in the left panel of Figure 4. Due to the large difference of the atomic number, the AO planes result in much stronger signal intensity, and thus have more robust signal-to-noise ratio than the BO_2 planes. Therefore, the thickness of LSMO can also be estimated by the intensity variations of the AO planes. In PTO and STO, the intensity is homogeneous; however, it varies slightly in the LSMO layer. The slight variation may possibly result from the anion intermixing and the effect of interfacial strain. On the basis of intensity of HAADF image, the thickness is estimated as about 5 unit cells, consistent to the result of the EELS analysis.

We note that the LSMO layer in most cases has a wedge shape at the hillock feet (see Figures 2(a), 2(b), and 3). This geometric feature leads to unit cell steps at the interface to the PTO film. The results of thickness obtained by EELS-stack imaging technique suffer from an error of a half unit cell. From the comparison of the EELS result with HAADF, it is practical and facile to determine the thickness of LSMO layer by using the intensity profile of HAADF image. Considering the broad DW shown in Figure 3, the line profiles are investigated for both sides (see rectangle windows with integration width of ~3.93 nm) around the DW as shown in the left and right panels of Figure 3. It can be seen that the LSMO layer is 8-unit-cell thick below D1 and 7-unit-cell thick below D2. The LSMO layer thickness at the DW position is between 7 and 8 unit cells.

Statistic investigation was performed on more than eight LSMO hillocks in order to study the domain formation and DW location in the PTO film depending on the thickness of the LSMO layer. Here, we only focus on the DW (e.g., left DW in Figure 2(b)) beneath which the LSMO layer possesses a limit thickness. The results are shown in Figure 5, obtained by using ABF/HAADF imaging (LSMO hillock edges 1–9) and HRTEM (hillock edge 10–16) techniques. It is evident that the DWs appear at positions where the LSMO layer has a thickness of about 8 unit cells. The obtained thickness of LSMO layer is found to be very close to that of the so-called "dead layer" (or critical thickness) in manganite ultrathin films,[35–37] at which the electrical and/or magnetic properties of (La,Sr)MnO_3 deviate greatly from those of the bulk. Huijben *et al*. reported a critical thickness for metallicity of 8 unit cells and for ferromagnetism of 3 unit cells in ultrathin $La_{0.7}Sr_{0.3}MnO_3$ films grown on STO (001) substrate;[35] Boschker *et al*. reported a critical thickness of ~10 unit cells for $La_{0.67}Sr_{0.33}MnO_3$ film grown on STO (110) substrate, below which an antiferromagnetic insulating phase appears.[36] This phase was related to the occurrence of a higher symmetric structural phase with an oxygen octahedral rotation pattern differing from that in the (La,Sr)MnO_3 bulk with R-3c symmetry.[36] Based on our results and the reported properties of (La,Sr)MnO_3 ultrathin film, we can conclude that a metal-to-insulator transition occurs at the thickness of below ~8 unit cells in the LSMO hillock feet. Interfacing to an insulator, domains form for lowering the system energy. The width of the domains determines the position of the DW over the length of the insulating LSMO layer. Controlling the shape of the LSMO hillocks provides a practical opportunity to engineer the DWs in ferroelectric films. It also provides very suitable samples for studying the structural transition and the electrical and/or magnetic inhomogeneity in such material system.

In summary, the formation of 180° ferroelectric domains in the PTO film, grown on top of the LSMO submicron hillocks on Nb-STO substrate, exhibits strong dependence on the thickness of underlying LSMO. A characteristic maximum thickness of about 8 unit cells for inducing ferroelectric 180° domain structures has been determined by line profiles of ABF/HAADF images combined with EELS. The thickness variation of the LSMO submicron hillocks provides an opportunity for studying the role of structural inhomogeneity together with the electrical and magnetic phase separation in doped manganite films, and shows potential application in manipulating the position and density of the ferroelectric domains and DWs, which are considered as active device elements in future nanoelectronics.

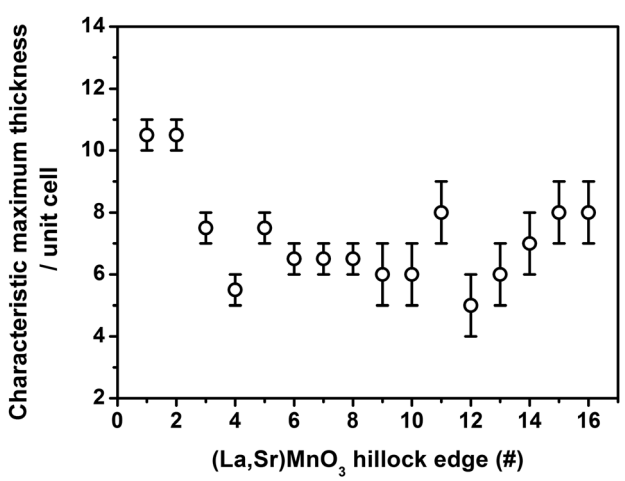

FIG. 5. Statistic measurement of the characteristic maximum thickness of LSMO layer by using HAADF/ABF imaging (hillock edges 1–9) and high resolution TEM (edges 10–16) from $\langle 100\rangle_{Nb\text{-}STO}$ and $\langle 110\rangle_{Nb\text{-}STO}$ FIB lamellae.

The authors thank Doris Meertens for specimen preparation by focused ion beam milling, Dr. Emrah Yücelen (FEI Company, the Netherlands), and Dr. Markus Heidelmann for introduction of the ABF imaging and StripeSTEM setups, and Dr. Alessio Morelli for the PFM investigation of the sample.

[1]A. S. Bhalla, R. Y. Guo, and R. Roy, Mater. Res. Innovations **4**, 3–26 (2000).
[2]N. A. Benedek and C. J. Fennie, J. Phys. Chem. C **117**, 13339–13349 (2013).
[3]J. G. Bednorz and K. A. Müller, Rev. Mod. Phys. **60**, 585–600 (1988).
[4]R. Micnas, J. Ranninger, and S. Robaszkiewicz, Rev. Mod. Phys. **62**, 113–171 (1990).
[5]M. B. Salamon and M. Jaime, Rev. Mod. Phys. **73**, 583–628 (2001).
[6]R. Ramesh and N. A. Spaldin, Nat. Mater. **6**, 21–29 (2007).
[7]G. Catalan and J. F. Scott, Adv. Mater. **21**, 2463–2485 (2009).
[8]M. Dawber, K. M. Rabe, and J. F. Scott, Rev. Mod. Phys. **77**, 1083–1130 (2005).
[9]H. J. Snaith, J. Phys. Chem. Lett. **4**, 3623–3630 (2013).
[10]A. Morelli, S. Venkatesan, B. J. Kooi, G. Palasantzas, and J. Th. M. De Hosson, J. Appl. Phys. **105**, 064106 (2009).

[11]C. L. Jia, K. W. Urban, M. Alexe, D. Hesse, and I. Vrejoiu, Science **331**, 1420–1423 (2011).
[12]I. Vrejoiu, A. Morelli, F. Johann, and D. Biggemann, Appl. Phys. Lett. **99**, 082906 (2011).
[13]Y. Kim, S. Jesse, A. Morelli, S. V. Kalinin, and I. Vrejoiu, Appl. Phys. Lett. **103**, 192901 (2013).
[14]L. Jiang, W. S. Choi, H. Jeen, T. Egami, and H. N. Lee, Appl. Phys. Lett. **101**, 042902 (2012).
[15]S. K. Streiffer, J. A. Eastman, D. D. Fong, C. Thompson, A. Munkholm, M. V. R. Murty, O. Auciello, G. R. Bai, and G. B. Stephenson, Phys. Rev. Lett. **89**, 067601 (2002).
[16]D. D. Fong, G. B. Stephenson, S. K. Streiffer, J. A. Eastman, O. Auciello, P. H. Fuoss, and C. Thompson, Science **304**, 1650–1653 (2004).
[17]I. Kornev, H. X. Fu, and L. Bellaiche, Phys. Rev. Lett. **93**, 196104 (2004).
[18]S. Prosandeev and L. Bellaiche, Phys. Rev. B **75**, 172109 (2007).
[19]P. Aguado-Puente and J. Junquera, Phys. Rev. Lett. **100**, 177601 (2008).
[20]A. Lubk, S. Gemming, and N. A. Spaldin, Phys. Rev. B **80**, 104110 (2009).
[21]A. V. Goltsev, R. V. Pisarev, Th. Lottermoser, and M. Fiebig, Phys. Rev. Lett. **90**, 177204 (2003).
[22]C. L. Jia, S. B. Mi, K. Urban, I. Vrejoiu, M. Alexe, and D. Hesse, Nat. Mater. **7**, 57–61 (2008).
[23]P. Gao, C. T. Nelson, J. R. Jokisaari, S. H. Baek, C. W. Bark, Y. Zhang, E. G. Wang, D. G. Schlom, C. B. Eom, and X. Q. Pan, Nat. Commun. **2**, 591 (2011).
[24]P. Gao, J. Britson, J. R. Jokisaari, C. T. Nelson, S. H. Baek, Y. R. Wang, C. B. Eom, L. Q. Chen, and X. Q. Pan, Nat. Commun. **4**, 2791 (2013).
[25]C. T. Nelson, B. Winchester, Y. Zhang, S. J. Kim, A. Melville, C. Adamo, C. M. Folkman, S. H. Baek, C. B. Eom, D. G. Schlom, L. Q. Chen, and X. Q. Pan, Nano Lett. **11**, 828–834 (2011).
[26]J. Seidel, L. W. Martin, Q. He, Q. Zhan, Y. H. Chu, A. Rother, M. E. Hawkridge, P. Maksymovych, P. Yu, M. Gajek, N. Balke, S. V. Kalinin, S. Gemming, F. Wang, G. Catalan, J. F. Scott, N. A. Spaldin, J. Orenstein, and R. Ramesh, Nat. Mater. **8**, 229–234 (2009).
[27]J. Seidel, P. Maksymovych, Y. Batra, A. Katan, S. Y. Yang, Q. He, A. P. Baddorf, S. V. Kalinin, C. H. Yang, J. C. Yang, Y. H. Chu, E. K. H. Salje, H. Wormeester, M. Salmeron, and R. Ramesh, Phys. Rev. Lett. **105**, 197603 (2010).
[28]S. Y. Yang, J. Seidel, S. J. Byrnes, P. Shafer, C. H. Yang, M. D. Rossell, P. Yu, Y. H. Chu, J. F. Scott, J. W. Ager III, L. W. Martin, and R. Ramesh, Nat. Nanotechnol. **5**, 143–147 (2010).
[29]J. Seidel, D. Y. Fu, S. Y. Yang, E. Alarcón-Lladó, J. Q. Wu, R. Ramesh, and J. W. Ager III, Phys. Rev. Lett. **107**, 126805 (2011).
[30]N. Balke, B. Winchester, W. Ren, Y. H. Chu, A. N. Morozovska, E. A. Eliseev, M. Huijben, R. K. Vasudevan, P. Maksymovych, J. Britson, S. Jesse, I. Kornev, R. Ramesh, L. Bellaiche, L. Q. Chen, and S. V. Kalinin, Nat. Phys. **8**, 81–88 (2012).
[31]G. Catalan, J. Seidel, R. Ramesh, and J. F. Scott, Rev. Mod. Phys. **84**, 119–156 (2012).
[32]M. Heidelmann, J. Barthel, and L. Houben, Ultramicroscopy **109**, 1447–1452 (2009).
[33]R. Ishikawa, E. Okunishi, H. Sawada, Y. Kondo, F. Hosokawa, and E. Abe, Nat. Mater. **10**, 278–281 (2011).
[34]J. S. Jeong, P. Ambwani, B. Jalan, C. Leighton, and K. A. Mkhoyan, ACS Nano **7**, 4487–4494 (2013).
[35]M. Huijben, L. W. Martin, Y. H. Chu, M. B. Holcomb, P. Yu, G. Rijnders, D. H. A. Blank, and R. Ramesh, Phys. Rev. B **78**, 094413 (2008).
[36]H. Boschker, J. Kautz, E. P. Houwman, W. Siemons, D. H. A. Blank, M. Huijben, G. Koster, A. Vailionis, and G. Rijnders, Phys. Rev. Lett. **109**, 157207 (2012).
[37]J. Z. Sun, D. W. Abraham, R. A. Rao, and C. B. Eom, Appl. Phys. Lett. **74**, 3017–3019 (1999).